Chapter-4

Interface engineered polymer nanocomposite thin-films for optoelectronic applications

4.1 Synthesis methodology

4.1.1 Materials

Zinc acetate dihydrate ACS reagent ≥ 98%, Ethanol absolute ≥ 99.8%, Diethanolamine reagent grade ≥ 98.0%, PMMA-Poly(methacrylic acid methyl ester) average M_w ~120,000 by GPC were purchased from Sigma Aldrich. Sodium hydroxide pellets ACS reagent > 99% were purchased from Thermo fisher scientific. Toluene ACS reagent > 99.5 % was purchased from Merck Millipore.

4.1.2 Fabrication of ZnO/PMMA hybrid thin films

1. **Surface treatment of Si wafers:** Prior to spin coating, the silicon substrates were thoroughly treated to remove any organic impurities and obtain a homogenous surface. First, they were immersed in Piranha solution (3:1 H_2SO_4 : H_2O_2) for half an hour and then rinsed twice with DI water. Then, sonication was carried out for 10 min in isopropyl alcohol and finally the surface was plasma treated (Diener plasma surface technology) for 10 min under 0.5 mbar pressure and 20-watt excitation power.
2. **Preparation of precursor solution:** 150 mg of PMMA was dissolved in 30 ml of toluene to prepare a 0.5 wt. % solution which was kept overnight on a magnetic stirrer at room temperature. The solution was divided into sets of equal volume and appropriate amount of nano ZnO suspension with empirically calculated wt. ratios was added to prepare different precursors with varying nano-filler %. The resulting nanocomposite precursor solution was ultrasonicated for 4 hours to ensure homogenous dispersion of nano-fillers.
3. **Programmed Spin coating:** The spin coater was programmed for a coating duration of 30 seconds and a coating speed of 3000 rpm. A fixed volume of 100 microliters was used for both pure PMMA and nanocomposite films. Post coating, the thin films were thermally treated on a hot plate for 1 hour at 100ºC to ensure stability and complete evaporation of the solvent.

4.2 Experimental methods

SPIN COATING- Pristine PMMA and PMMA/ZnO nanocomposite thin films were spin-coated onto Si wafers (1*1 cm) using Spin NXG-P2 spin coating system by Apex instruments. The Si wafers underwent a surface plasma treatment (Deiner electronic) using oxygen plasma at very low pressure for 10 minutes.

FESEM- Microstructural investigation of thin film's surface and interface was performed with Sigma 300 Field Emission Scanning Electron Microscope by Zeiss. The sample was sputtered with a thin conductive layer of gold prior to imaging to avoid charging of the insulating polymer by electron beam. Data was acquired varying the accelerating voltage between 5 and 15 kV.

AFM- Surface topography and phase analysis were obtained using Park XE7 (South Korea) Atomic Force Microscope operated in contact mode for height profile and tapping mode for phase images. Surface roughness analysis and 3D topography was acquired from AFM data with the help of Gwyddion software.

XPS- Surface and interfacial chemistry of nanocomposite thin films was studied using K-alpha X-ray Photoelectron Spectrometer system by Thermo Scientific equipped with Al Kα micro focussed monochromator and 180º double focusing hemispherical analyzer with 128-channel detector.

PLE- Photoluminescence emission spectra of ZnO/PMMA hybrids was acquired in the wavelength range 400-800 nm using Fluorescence Spectrophotometer F-4600 by Hitachi with excitation and emission slit width 10 nm and PMT voltage 700 V.

4.3 Results & Discussion

4.3.1 Microstructural Surface and Interfacial studies

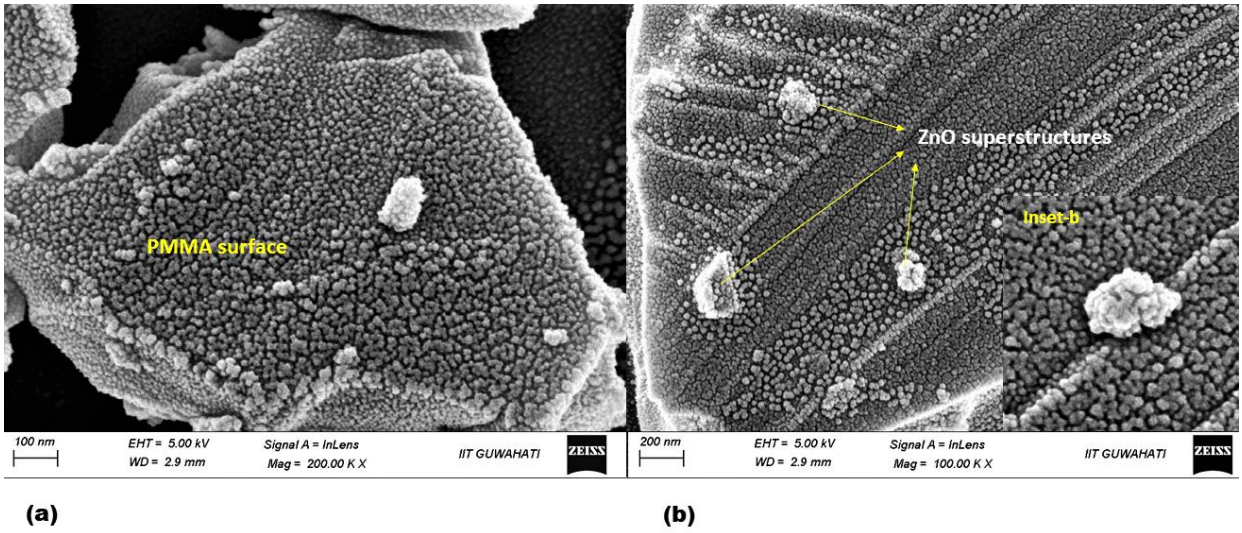

Fig 4.1- (a) FE-SEM image showing the microstructure of PMMA surface & (b) Homogenously distributed ZnO nanoclusters in PMMA matrix (0.25 wt%) with absence of any agglomerates, (Inset-b) Thin PMMA layer covered surface of a porous self-assembled ZnO nanocluster.

High resolution FE-SEM images (Fig 4.1) reveal the porous microstructure of spin-coated PMMA. The surface consists of nano-sized PMMA grains with a uniform size distribution, low roughness and an overall smooth morphology which is consistent with the AFM roughness measurements (RMS roughness : 0.247 nm). The incorporation of ZnO nanostructures didn't affect the morphology of PMMA surface owing to superior interfacial interactions mediated by strong chemical bonds between diethanolamine modified ZnO surface and PMMA chains resulting in a defect-free, highly stable interface with consistent properties. The size of nanostructures embedded in PMMA matrix is slightly larger than that of HRTEM measurement which is attributed to a thin PMMA coating on modified ZnO surface and not because of agglomeration since no agglomeration was observed in the AFM topography images of nanocomposite films. Close investigation of embedded ZnO nanoclusters reveal their three dimensional morphology which is strongly correlated to the HRTEM observations. It is composed of self-assembled nano-crystallites, with sizes in quantum regime (<10nm), forming a pompon-like structure. The nanoclusters owing to their unique morphology are characterized by high porosity and enhanced effective surface area as compared with bulk nanoparticles. The self-assembly possibly induced a large number of interfacial defects which could be the reason for sharp, highly intense green luminescence observed in the PL emission spectra.

The effect of increasing the nano-filler loading percentage is presented in Fig 4.2. ZnO nanocluster loading at 2 wt% did not induce any microstructural changes and the thin film had a highly homogenous and uniform surface. However, high-resolution micrographs of 5 wt% nanocomposites depict few polymer-encapsulated agglomerates. This was possibly induced due to the increase in viscosity of the polymer which prevented a smooth distribution of the precursor solution on the substrate during the spin coating process.

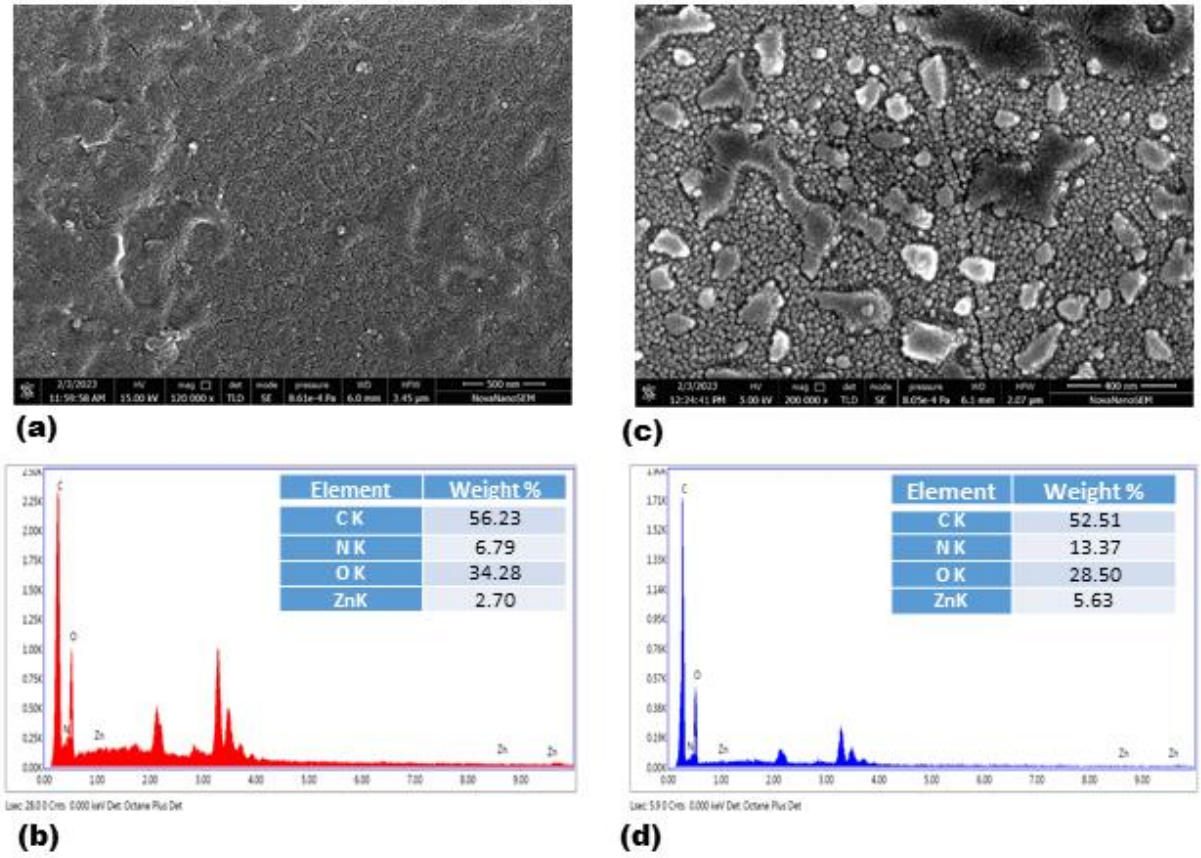

Fig 4.2- (a,c) FE-SEM images of 2 wt% and 5 wt% nanocomposite thin films respectively.

(b,d) EDX spectra and corresponding elemental composition of 2 wt% and 5 wt% nanocomposite thin films respectively. (Unmarked peaks correspond to the ITO coated substrate)

Fig 4.3 illuminates the elemental distribution of a selected area (Fig 4.4-a) of 2 wt% nanocomposite thin film. Element map of C and O are densely packed due to higher contribution from PMMA (~98 wt %) and the Zn map which is representative of ZnO distribution in the thin film suggests highly uniform dispersion of nanostructures.

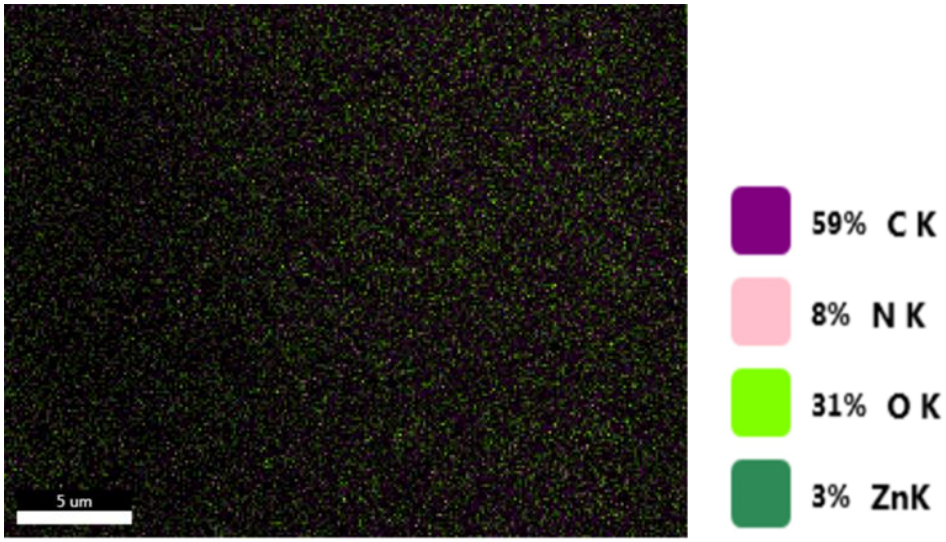

Fig 4.3- Composite element map of 2 wt% ZnO/PMMA hybrid along with elemental composition of C,O,N and Zn.

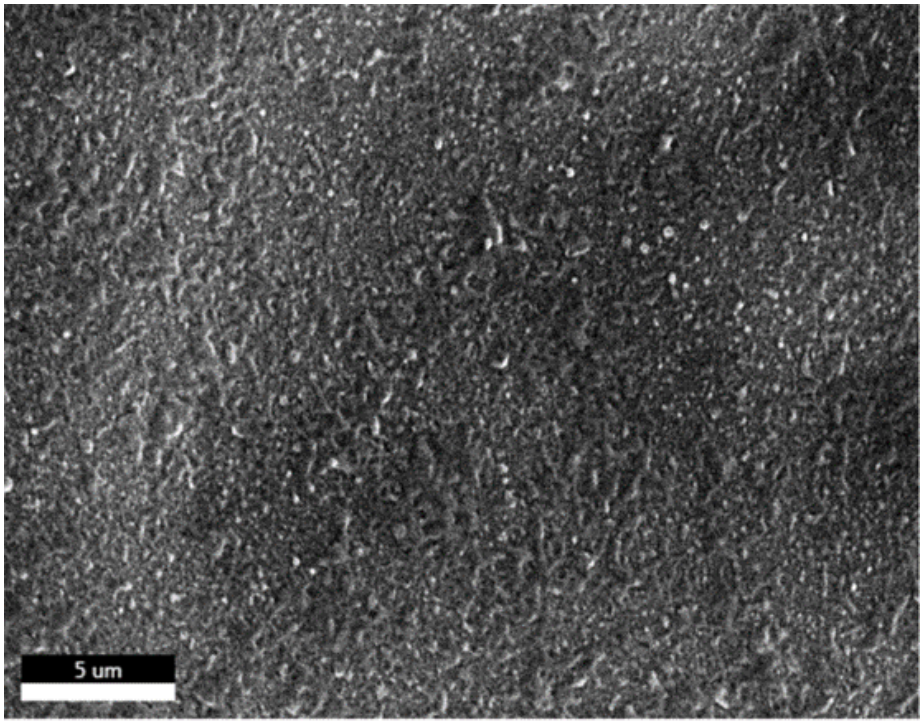

Fig 4.4 : FESEM micrograph of 2 wt % ZnO/PMMA nanocomposite thin film. The white dots in the image represent the ZnO distribution (Element map fig 4.5-c)

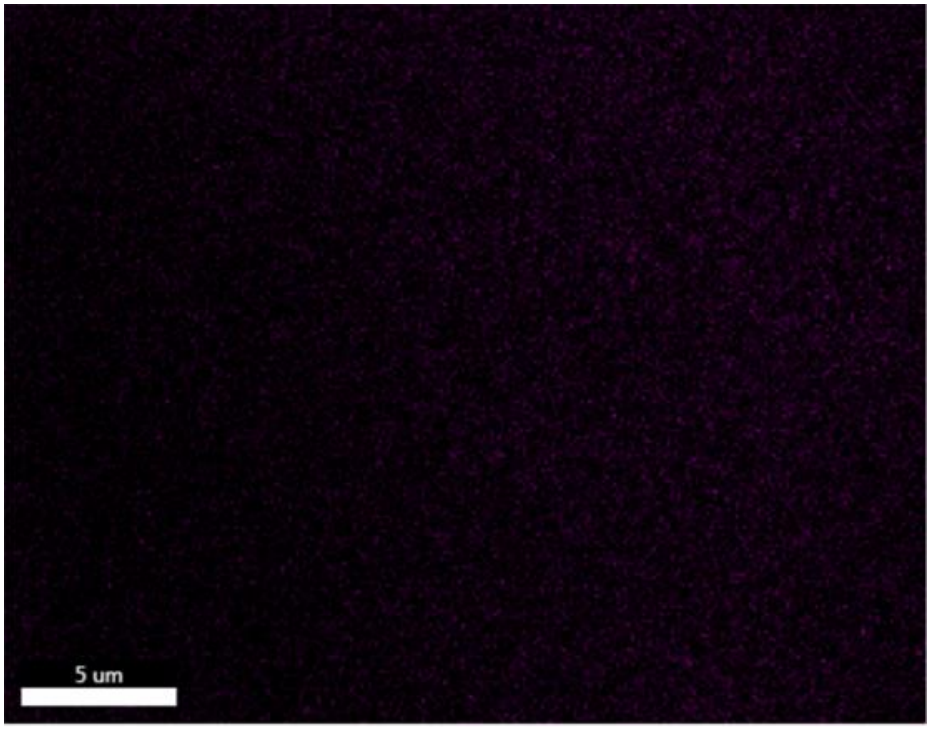

Fig 4.5-a : Elemental distribution of C in Fig 4.4

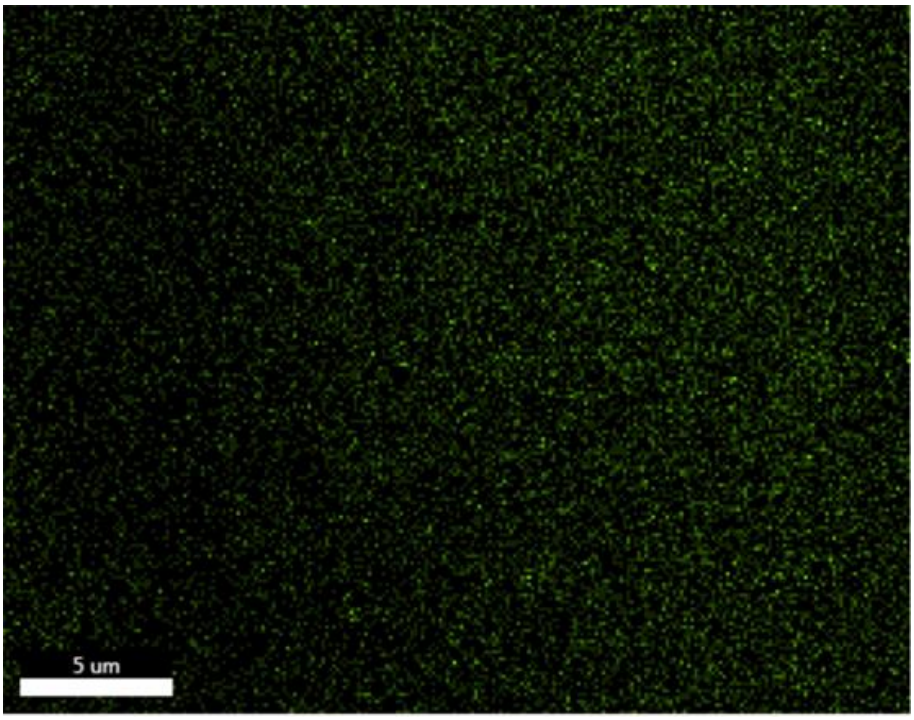

Fig 4.5-b : Elemental distribution of O in Fig 4.4

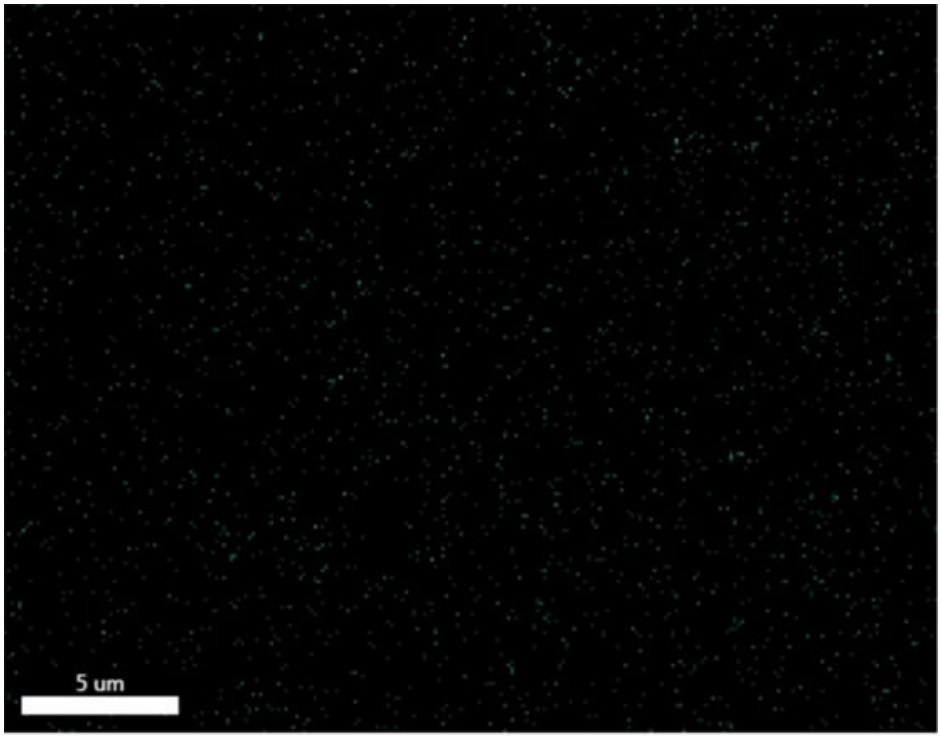

Fig 4.5-c : Elemental distribution of Zn in Fig 4.4

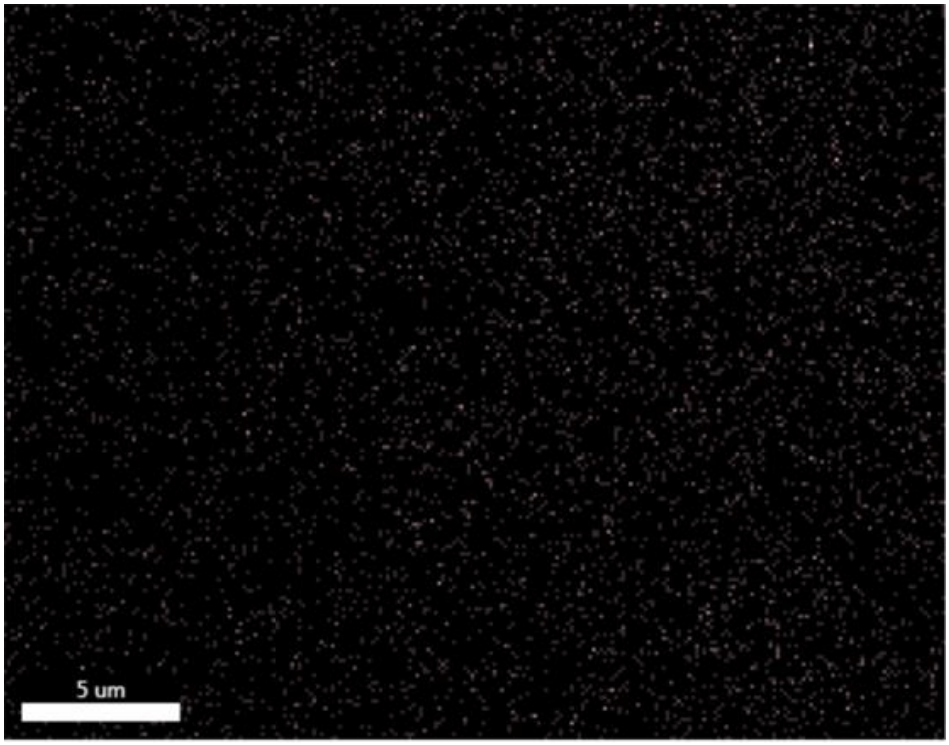

Fig 4.5-d : Elemental distribution of N in Fig 4.4

4.3.2 Topography and surface roughness measurements

Fig 4.6 (a, b) represent the surface topography and phase images of pure PMMA film. Results from both the techniques indicate a smooth and homogenous surface without any sharp contrast in height or phase angle. Spin coating at a high rotation speed and low polymer concentration led to the formation of films with low surface roughness and high homogeneity as evident from the color distribution of AFM images. Fig 4.6 (d, e) depicts the surface topography and phase images of ZnO mesocrystal embedded PMMA film. Height profile images indicate a homogenous background with uniform thickness as represented by the smooth darker shades and uniformly distributed protrusions coded in the brighter shades. The protrusions with an avg. height of around 50 nm could be identified as the ZnO nanoclusters but since the topographic images only give information based on the height variation, they alone cannot be used to assure the presence and position of nanostructures. Phase imaging which produces color profiles depending on the stiffness of constituent phases was used to complement the topographical analysis. The position of bright spots in phase images exactly overlaps with the tall features in topography images thus confirming the presence of ZnO nanostructures. The size of nanostructures from AFM images is in excellent agreement with HRTEM and DLS size measurements. Maximum height of the color bar was 61.8 nm suggesting no agglomeration of the ZnO phase owing to the high stability of self-assembled mesocrystals. Surface capping with a di-functional organic ligand highly enhanced the compatibility between polymer and inorganic phase as evident from the uniform distribution of nanoparticles in the polymer matrix.

Physical interactions between the nanostructures and PMMA matrix were studied from the three dimensional representation of the nanocomposite surface. Surface roughness was induced in the matrix due to interactions with ZnO nanoparticles as evident from the topographical variations at the interface. Smaller-sized particles ~ 30 nm had lesser impact on the polymer surface while larger ~50 nm particles strongly altered the interface region inducing large depth variations as evident from the locally concentrated darker regions around them. It was concluded that the local surface properties of nanocomposite films such as texture, roughness could be tuned by varying the size and morphology of nano fillers. The interfacial interactions and dispersion state of nanofillers in organic matrix is highly dependent on the surface functionality of nanostructures where small chain ligands like diethanolamine are extremely effective in capping and bridging mechanisms.

Surface roughness profile

Fig 4.6 (c, f) represent the surface roughness data acquired along a line profile. The values of key parameters used to quantify the surface roughness of pure PMMA and PMMA nanocomposite film are listed in Table 4.1. Pure PMMA film had an extremely low average roughness and RMS roughness with values 0.179 nm and 0.247 nm respectively owing to the smooth texture of spin-coated thin films. Even with the inclusion of ZnO nanostructures the values remained on the lower side with average and RMS roughness values of 2.90 nm and 3.94 nm respectively which suggests that the spin-coating method is highly efficient in producing smooth and homogenous films with minimal irregularities. Film deposition at a higher rotation speed assisted in the uniform dispersion of nanoparticles as evident from the roughness profile of PZ-3 film where roughness peaks along the selected line profile highlight evenly spaced nanoparticles. Advance roughness parameters such as Skewness and Kurtosis were also computed with the help of Gwyddion software.

Skewness, which is the measure of symmetry in a data distribution was computed by the relation:

$$\mathbf{R_{sk}} = \frac{\sum_{i=1}^{N}(Y_i - \overline{Y})^3 / N}{s^3} \qquad (4.1)$$

Skewness value for pure PMMA film was -0.854. The values close to 0 represent a symmetric data set and the negative sign is indicative of left skewness. Nanocomposite film had a slightly larger positive skewness of 1.564 due to the topographical contrast between polymer and ZnO phase.

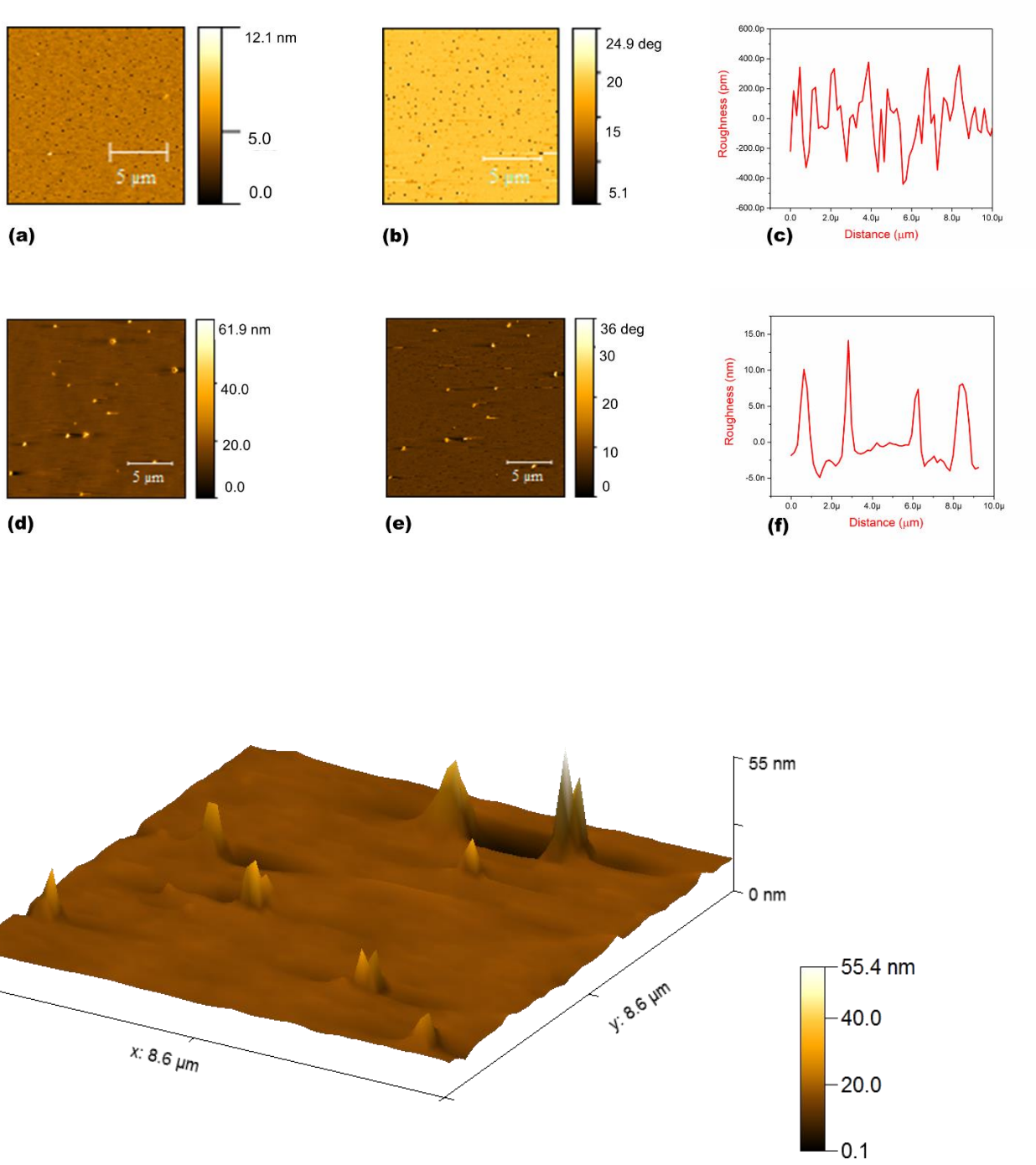

Fig 4.6- Top panel: (a & d) Surface topography, (b & e) Phase images, (c & f) Surface roughness profiles of Pristine PMMA (P1) and PMMA/ ZnO nanocomposite (PZ-3) thin films respectively. Bottom panel: Three dimensional surface topographic profile of 0.5 wt% PMMA/ZnO nanocomposite thin film generated by Gwyddion software.

Kurtosis, which measures whether the data is heavy-tailed or light-tailed relative to a normal distribution was computed by the relation:

$$\mathbf{R_{ku}} = \frac{\sum_{i=1}^{N}(Y_i - \overline{Y})^4 / N}{s^4} \quad (4.2)$$

The kurtosis values for P-1 and PZ-3 films were 5.739 and 5.028 respectively which is indicative of a moderate kurtosis since the value for a standard normal distribution is 3.

In equations (1) and (2) Y_i and $\overline{Y}$ represent i^{th} reading and mean respectively, s is the standard deviation and N is the number of data points.

	Roughness average (R_a)	**Root mean square roughness (R_q)**	**Avg. max height of the profile (R_z)**	**Skewness (R_{sk})**	**Kurtosis (R_{ku})**
P1	0.179 nm	0.247 nm	0.911 nm	-0.854	5.739
PZ3	2.905 nm	3.945 nm	15.717 nm	1.564	5.028

Table 4.1- Advance surface roughness parameters computed for P1- Pristine PMMA film and PZ3- 0.5 wt% PMMA/ZnO nanocomposite film.

4.3.3 Surface and Interfacial Chemistry (XPS)

Core levels of XPS were used to probe the chemical composition and bonding states of different elements present on the surface of nanocomposite film. Owing to the high surface sensitivity, XPS proves to be an extremely efficient technique for exploring the interfacial interactions and chemical stability of complex hybrid surfaces composed of long-chain polymers, short-chain organic ligands and inorganic nanostructures interacting via various mechanisms such as covalent, ionic and hydrogen bonding.

We studied the surface of 0.1 wt.% ZnO/PMMA nanocomposite film and the binding energy profiles in C1s, O1s, N1s and Zn2p regions are presented in Fig 4.7.

C1s spectra was deconvoluted with respect to four major peaks of PMMA [171] and an additional peak from covalent bonding between PMMA chains and DEA moeity. The lowest energy peak at 284.51 eV with maximum area under the curve was assigned to aliphatic carbon (C-C/C-H). The peak at 285.78 eV and 286.90 eV were observed from C-O and C=O respectively. The interfacial bonding between polymer and surfactant contributed to the N-C=O peak at 288.51 eV thus establishing the formation of Class-II hybrids. The peak from carboxylate group O-C=O was observed at higher binding energy, 289.13 eV as compared to bulk PMMA (289 eV). This significant shift could be attributed to the hydrogen bonding between unbonded oxygen from carboxyl group and diethanolamine capped ZnO surface. The resulting chemical interaction between the inorganic and polymer phase could render high stability to the surface of nanocomposite films.

The resolved O1s spectra depicted the characteristic Zn-O peak at 530.4 eV [172] with very low intensity owing to the extremely low nanofiller percentage. The computed atomic percentage of Zn from the XPS survey was 0.09 % which agrees with the empirically calculated value. The other peaks observed in O1s region were C-O and C=0 at 533.7 and 532.4 respectively. [173] N1s region exhibited a major peak at 399.6 eV corresponding to the N-H bond from diethanolamine. A minor peak was also observed at 401.1 eV which could be attributed to the covalent bond (N-C=O) between PMMA chains and diethanolamine molecules on ZnO surface thus providing a quantitative evidence of the chemical interactions at the interface. The core levels of the Zn2p orbital exhibited a doublet peak due to the spin-orbit splitting or j-j coupling. For 2p orbital, we have n=2 and l=1 and s has values +1/2 and -1/2. We can calculate the total angular momentum j:

$$j=l+s \tag{4.3}$$

where l is the orbital angular momentum and s is the spin angular momentum**.**

So, j will have two values 1/2 and 3/2 corresponding to 2p1/2 and 2p3/2 peaks which were positioned at 1045.2 and 1022.4 eV respectively [174] with spin-orbit splitting energy value of 22.8 eV. The doublet peak areas have a fixed ratio determined by the degeneracy **(2j+1)** of different levels. 2p3/2 has a degeneracy of 4 i.e. it can accommodate 4 electrons whereas 2p1/2 with degeneracy 2 can occupy only 2 electrons. Hence the area ratio of 2p peaks should be 2:1 which is clearly evident from the XPS spectra. (Fig 4.7(b))

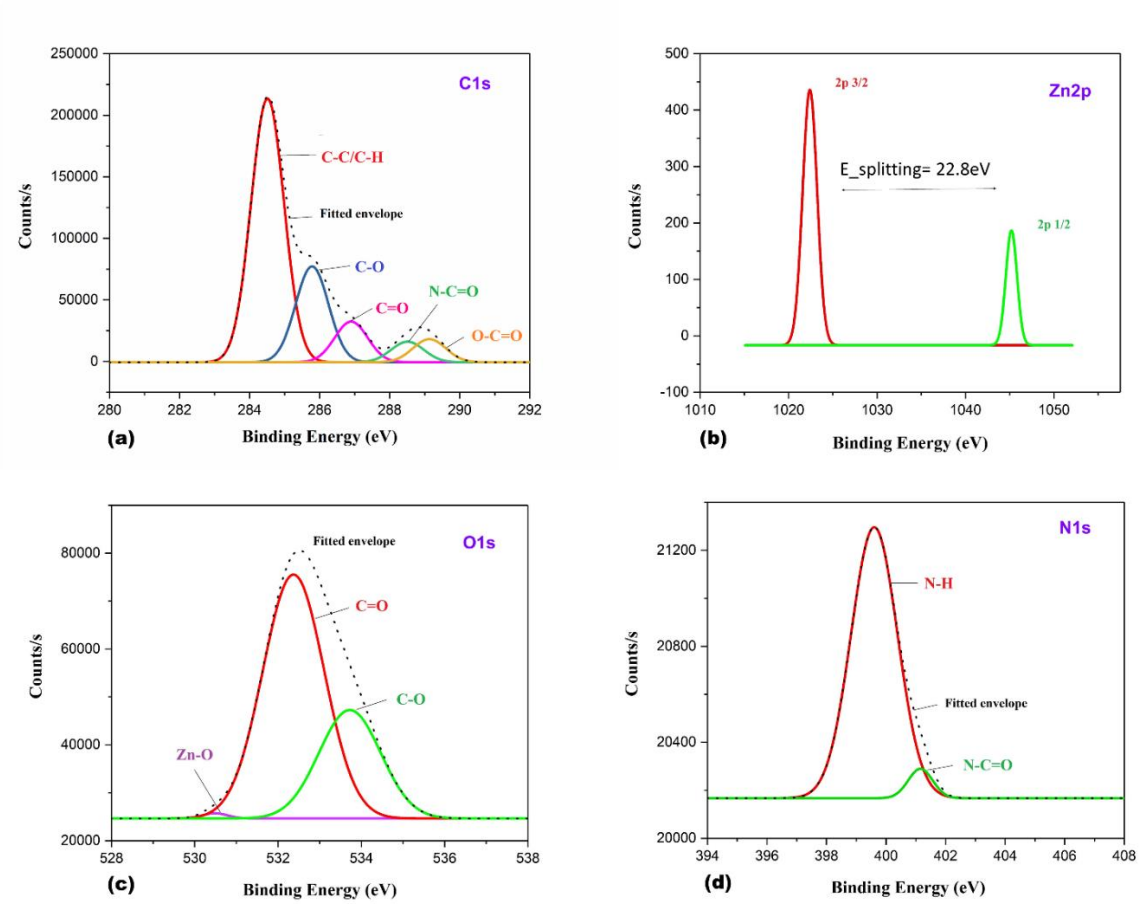

Fig 4.7- High resolution XPS spectra of 0.1 wt % PMMA/ZnO nanocomposite thin film in (a) C1s region with characteristic PMMA peaks, (b) Zn2p region depicting spin-orbit splitting in 2p levels, (c) O1s region with characteristic Zn-O peak and (d) N1s region indicating covalent bond between PMMA and DEA molecules on ZnO surface.

4.3.4 Optoelectronic characteristics of nanocomposite thin films

- **UV shielding properties**

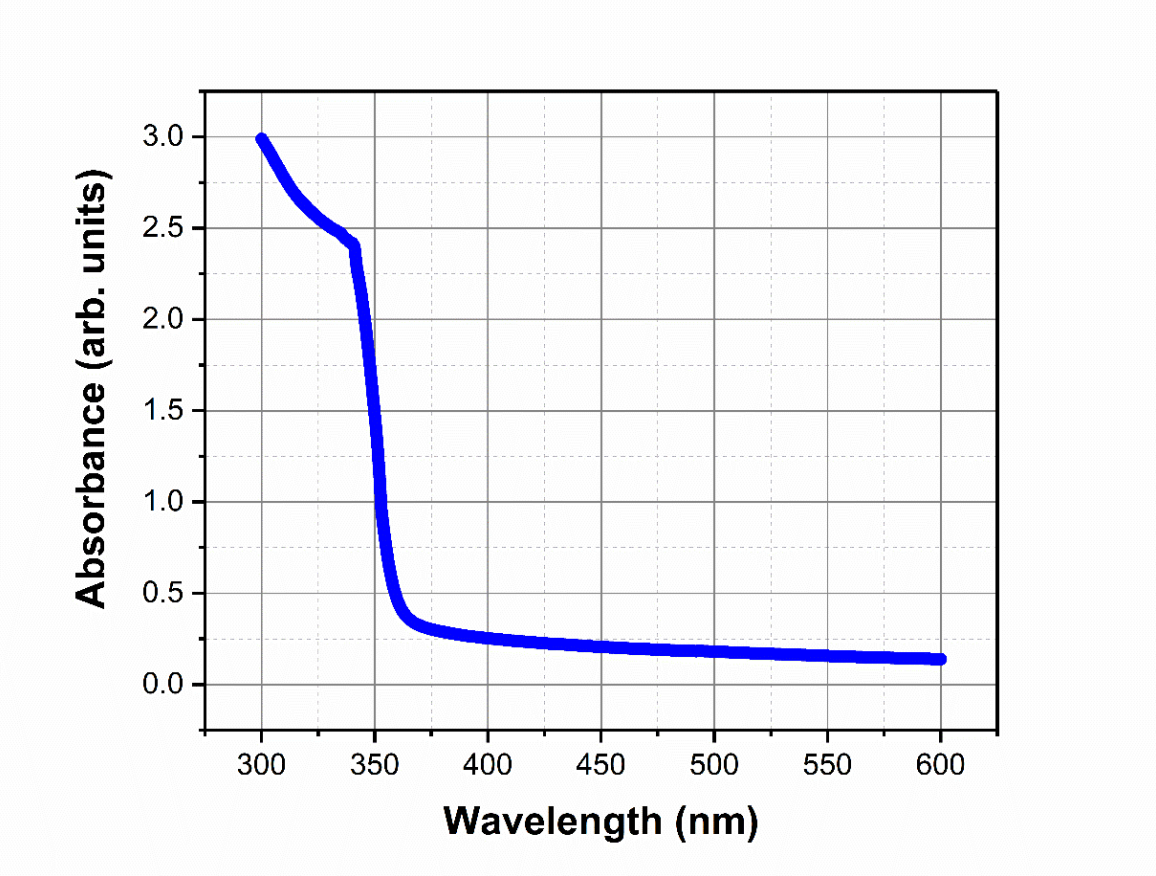

Fig 4.8- UV-Vis spectra of 2 wt % ZnO/PMMA hybrid with 85-90 % transparency in the visible region.

The UV-Vis spectra of the nanocomposite film (Fig 4.8) displays the absorption peak at almost the same wavelength as the colloidal ZnO dispersion. The thin films exhibit excellent absorption characteristics ranging from 300nm to 360 nm which spans both the UV-A and UV-B spectrum which is considered harmful for both humans and natural resources such as plantations, water bodies, etc .Ultraviolet A (UVA) has a longer wavelength and is associated with skin aging while Ultraviolet B (UVB) has a shorter wavelength and is associated with skin burning. Additionally the nanocomposite films exhibited remarkable transparency in the visible region lying between 85-90 %, rendering them suitable for application as transparent conductive electrodes, UV shielding windows, active layer in energy conversion devices, etc.

- **Tuneable PL emission**

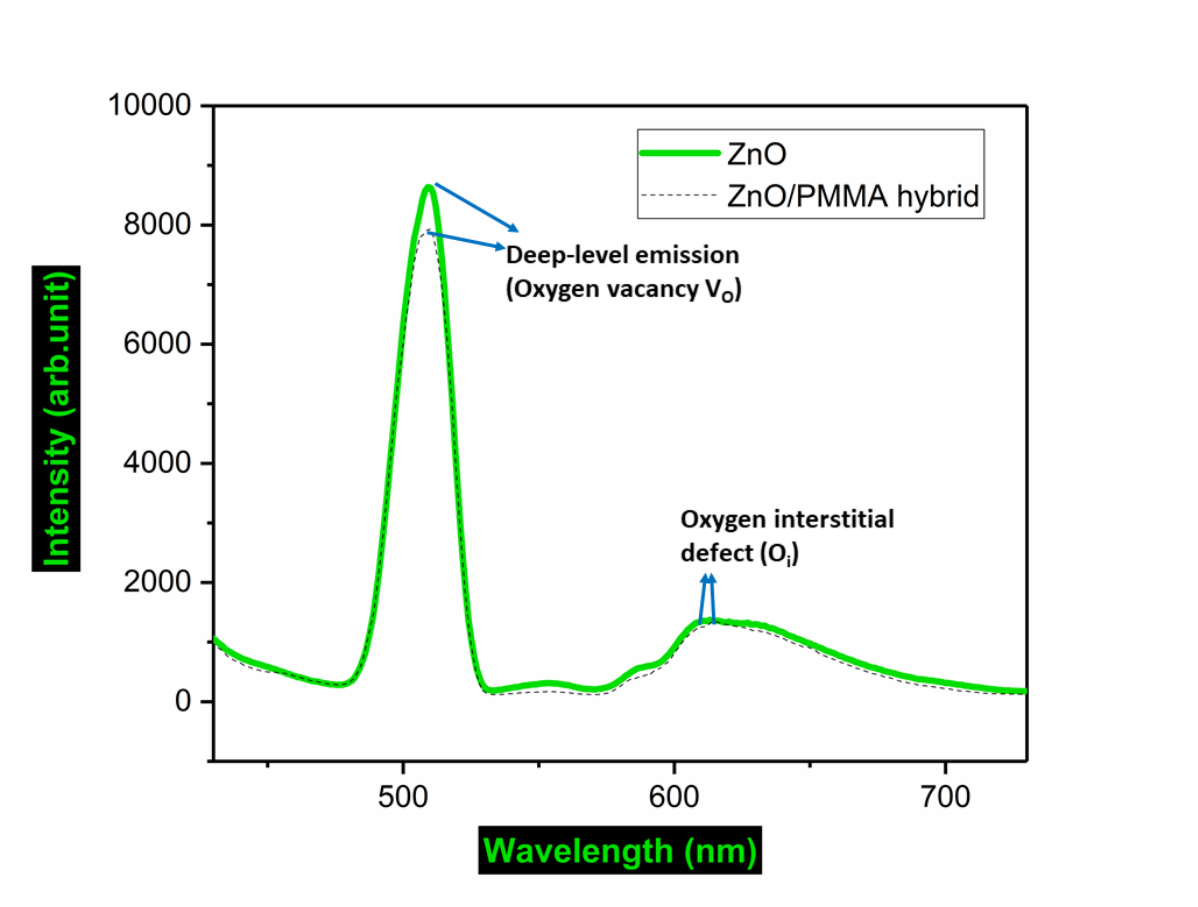

Fig 4.9- PL emission spectra of ZnO nanocluster and 2 wt% ZnO/PMMA hybrid depicting oxygen vacancy and oxygen interstitial surface defect induced green and orange emission bands respectively.

The photoelectric properties of 2 wt% ZnO/ PMMA nanocomposite are also presented in Fig 4.9 (dotted curve) for comparison. The PL emission of ZnO nanocluster in the hybrids had a slightly diminished intensity, possibly due to a decrease in the number of active defect sites owing to a thin PMMA layer. However, the PL peak positions didn't reflect any significant changes. The peaks of green and orange emission bands in the hybrids were observed at 509 nm and 613 nm respectively as compared to 510 nm and 610 nm for the ZnO nanocluster. Thus it can be concluded that the ZnO QD's preserved their quantum state in the hybrid since they display photoluminescence at the same wavelength. The result is also in agreement with the UV-Vis spectra of the nanocomposite which displays the absorption peak at almost the same wavelength as the colloidal ZnO dispersion. Hence, the optical analysis establishes that the

colloidal ZnO nanoclusters retain their chemical and molecular properties even after forming the hybrid.

Owing to the quantum dot size-dependent PL emission in ZnO nanoclusters, the visible range emission of the nanocomposite thin films could be tuned according to the size and morphology. The size-dependent photoluminescence characteristics could be utilized in fabricating flexible, tunable light-emitting diodes and fluorescence-based sensors, which would also benefit from the mechanical flexibility and durability of the polymer matrix.

4.4 Conclusion

The study demonstrates the synthesis and structure-property relationship of surface engineered nanocomposite thin-films composed of self-assembled ZnO nanocluster and optically transparent Polymethyl methacrylate matrix. Topographical and morphological surface studies by AFM and FE-SEM techniques confirmed the homogenous dispersion of nanofillers in the polymer matrix without any agglomeration which is necessary to prevent loss of transparency in the resulting hybrids. Surface roughness measurements gave extremely low roughness values, 0.179 nm and 2.905 nm for pristine PMMA and PMMA/ZnO nanocomposite thin films respectively. Eita et al. [135] obtained RMS roughness of nanocomposites ranging from 3.6 nm to 8.4 nm while Chen et al. [116] measured a RMS value 6.6 nm and avg. value 5.1 nm. A highly uniform, smooth morphology achieved in our work was attributed to several factors: (a) Surface plasma treatment of Si substrates, (b) High rpm spin-coating and (c) Excellent surface and interfacial properties bestowed by diethanolamine mediated chemical interactions between the organic and inorganic phase. XPS binding energy curves quantitatively studied the surface and interfacial chemistry of nanocomposite films. C1s spectra observed a shift in O-C=O peak attributed to hydrogen bonding between the carboxyl group and DEA-capped ZnO surface and an additional peak was observed in N1s spectra at 401.1 eV which could be attributed to the covalent bond (N-C=O) between PMMA chains and DEA molecules. The existence of chemical interactions at the interface provide evidence of the nanocomposite surface's excellent stability, which could efficiently enhance the performance and durability of thin film-based devices and coatings.